

## MATERIALS SCIENCE

# Altering the rate-determining step over cobalt single clusters leading to highly efficient ammonia synthesis

Sisi Liu, Mengfan Wang, Haoqing Ji, Xiaowei Shen, Chenglin Yan and Tao Qian\*

## ABSTRACT

Activation of high-energy triple-bonds of  $N_2$  is the most significant bottleneck of ammonia synthesis under ambient conditions. Here, by importing cobalt single clusters as strong electron-donating promoter into the catalyst, the rate-determining step of ammonia synthesis is altered to the subsequent proton addition so that the barrier of  $N_2$  dissociation can be successfully overcome. As revealed by density functional theory calculations, the  $N_2$  dissociation becomes exothermic over the cobalt single cluster upon the strong electron backdonation from metal to the  $N_2$  antibonding orbitals. The energy barrier of the positively shifted rate-determining step is also greatly reduced. At the same time, advanced sampling molecular dynamics simulations indicate a barrier-less process of the  $N_2$  approaching the active sites that greatly facilitates the mass transfer. With suitable thermodynamic and dynamic property, a high ammonia yield rate of  $76.2 \mu\text{g h}^{-1} \text{mg}_{\text{cat}}^{-1}$  and superior Faradaic efficiency of 52.9% were simultaneously achieved.

**Keywords:** nitrogen reduction reaction, rate-determining step, cobalt single cluster, mass transfer, molecular dynamics simulations

## INTRODUCTION

Ammonia ( $NH_3$ ) is widely considered as a critical chemical whether in agriculture or transportation [1,2], since it is the main ingredient for fertilizer production and a carbon-free energy storage intermediate with high-energy density [3]. Although an infinite nitrogen ( $N_2$ ) source from the atmosphere can be easily obtained, large scale ammonia production is hindered by the chemical stability of the  $N\equiv N$  bond (bond energy:  $940.95 \text{ kJ mol}^{-1}$ ) [4,5]. To date, the traditional Haber-Bosch process using transition metal as catalyst under drastic reaction conditions still dominates the industrial market of  $NH_3$  synthesis [6–8]. However, this typical strategy can only reach a relatively low conversion ratio ( $\sim 15\%$ ) and consumes nearly 5% of the world's natural gas [9,10]. The use of fossil fuels, at the same time, accounts for large quantities of  $CO_2$  generation into the atmosphere [11]. Therefore, a clean and sustainable strategy for  $NH_3$  production is urgently demanded for both the global population and energy.

The electrocatalytic  $N_2$  reduction reaction (NRR), using protons from water as the hydro-

gen source and powered by renewable electricity sources, is an alternative method to achieving  $N_2$  fixation under ambient conditions [12–16]. Theoretically, common mechanisms of the NRR start with  $N_2$  chemisorption on the catalyst's surface, followed by the cleavage of  $N\equiv N$  bond and consecutive proton addition to form  $NH_3$  [17]. Yet, strong bonding energy, high ionization potential, broad HOMO-LUMO gap as well as poor electron affinity of  $N_2$  do not favor any electron transfer process, and the  $N_2$  activation process is thus commonly considered as the rate-determining step [18,19]. A catalyst which features active sites with suitable energy and symmetry of orbitals is able to bind with  $N_2$  molecules through accepting electron density from, and backdonating to,  $N_2$  [20]. The backdonation, known as the  $\pi$  backbonding, strengthens the catalyst–nitrogen bond, weakens the  $N\equiv N$  bond, and thus contributes to lowering the energy barrier of  $N_2$  activation and positively shifting the rate-determining step [19]. This process could be enhanced by strong electron-donating ability, which enables the smooth electron transfer from the active site to the  $N_2$  antibonding  $\pi$ -orbitals,

College of Energy, Key Laboratory of Advanced Carbon Materials and Wearable Energy Technologies of Jiangsu Province, Soochow University, Suzhou 215006, China

\*Corresponding author. E-mail: [tqian@suda.edu.cn](mailto:tqian@suda.edu.cn)

Received 26 February 2020;  
Revised 17 May 2020; Accepted 28 May 2020

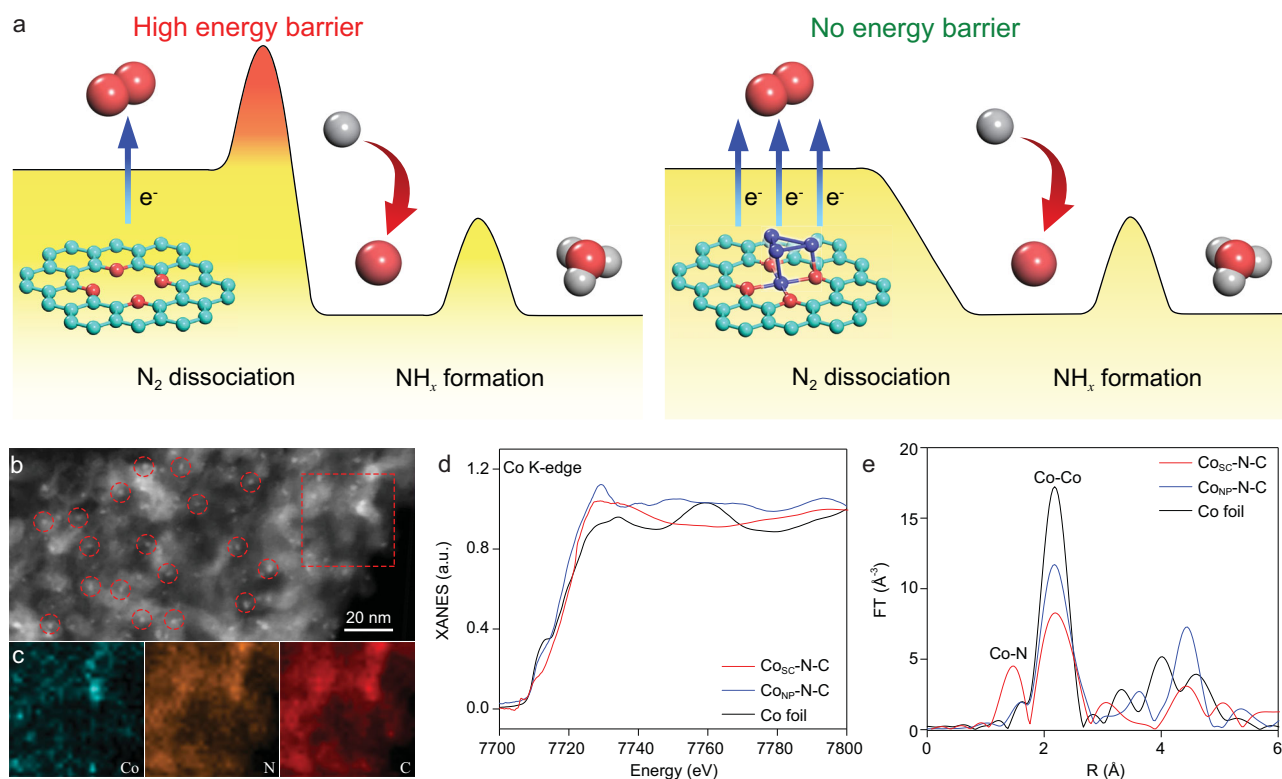


**Figure 1.** (a) Schematic illustration for the mechanism of enhanced NRR activity by introducing Co single cluster in nitrogen-doped carbon. The cyan, red, purple and gray spheres represent C, N, Co and H atoms, respectively. (b) Dark-field TEM image of  $\text{Co}_{\text{SC}}\text{-N-C}$  showing highly dispersed Co single clusters in the material and (c) corresponding element maps showing the distribution of Co (blue), N (orange) and C (red). (d) Co K-edge X-ray absorption near-edge structure (XANES) and (e) Fourier-transformed (FT)  $k^3$ -weighted extended X-ray absorption fine structure (EXAFS) spectra of  $\text{Co}_{\text{SC}}\text{-N-C}$ ,  $\text{Co}_{\text{NP}}\text{-N-C}$  and Co foil.

termed the electronic promoting effect [21–23], and further benefits the eventual  $\text{N}_2$  dissociation. Unfortunately, only very few catalysts reported to date can efficiently reduce the nitrogen activation barrier, leaving the ammonia production rate and Faradaic efficiency in low level [23–25]. Hence, searching for highly active catalysts that could alter the rate-determining step of electrochemical ammonia synthesis is still a challenging goal.

Herein, we successfully demonstrate that deliberately introducing cobalt single clusters as electron-donating promoter in nitrogen-doped carbon alters the rate-determining step of ammonia synthesis from  $\text{N}_2$  cleavage to proton addition (Fig. 1a). An excellent ammonia yield rate ( $76.2 \mu\text{g h}^{-1} \text{mg}_{\text{cat.}}^{-1}$ ) and a superior Faradaic efficiency (52.9%) were simultaneously obtained under ambient conditions. Isotopic labeling experiments and control experiments are combined to confirm that all the  $\text{NH}_3$  produced is from the  $\text{N}_2$  electrochemical reduction. Also, the catalyst is steady enough to suffer consecutive electrolysis recycle with negligible attenuation in the NRR activity and selectivity. Density functional theory (DFT) calculations reveal that  $\text{N}_2$  activation is transferred into a strong

thermodynamically exothermic process on cobalt single clusters, so that it is no longer the rate-determining step of ammonia synthesis. Instead, only small energy barriers exist upon  $\text{NH}_x$  formation in the whole nitrogen fixation process. Also, the approaching process of  $\text{N}_2$  molecules towards the single cluster sites is confirmed to be barrier-less by molecular dynamics (MD) simulations, which greatly favors the whole nitrogen reduction process. Altering the rate-determining step of nitrogen reduction effectively leads to a desirable NRR performance, and thus provides a powerful guidance for future design of catalysts.

## RESULTS AND DISCUSSION

### Characterization of the $\text{Co}_{\text{SC}}\text{-N-C}$ catalyst

The cobalt single clusters dispersed in nitrogen-doped carbon ( $\text{Co}_{\text{SC}}\text{-N-C}$ ) were fabricated and carefully characterized. The transmission electron microscopy (TEM) image (Supplementary Fig. 1) and dark-field TEM image (Fig. 1b) of  $\text{Co}_{\text{SC}}\text{-N-C}$  clearly show highly dispersed cobalt single clusters in the catalyst, with corresponding element

mapping (Fig. 1c) demonstrating the uniform distribution of Co superimposing with C and N. Using aberration corrected high-angle annular dark-field scanning transmission electron microscopy (HAADF-STEM) with sub angstrom resolution, the clusters are observed to be of small size with an average diameter of approximately 0.5 nm (Supplementary Fig. 2). The overall Co content in the Co<sub>SC</sub>-N-C is about 3.15 wt%, as determined by inductively coupled plasma optical emission spectrometry (ICP-OES) analysis. To highlight the specific role of cobalt single clusters, counterparts with cobalt nanoparticles (Co<sub>NP</sub>-N-C) and without metal (N-C) were also synthesized by replacing the Co<sup>2+</sup>/Zn<sup>2+</sup> mixture with single Co<sup>2+</sup> and Zn<sup>2+</sup>, respectively, under otherwise identical conditions (Supplementary Figs 3 and 4). As shown in the X-ray powder diffraction (XRD) patterns (Supplementary Fig. 5), Co<sub>NP</sub>-N-C exhibits distinct metallic cobalt diffraction, whereas the cobalt single clusters in Co<sub>SC</sub>-N-C exist as amorphous phase. The increased content of Co accounts for the improved graphitization degree, as evaluated by the Raman spectra (Supplementary Fig. 6).

To confirm the chemical state of Co species in different samples, X-ray absorption fine structure (XAFS) measurements were conducted with Co foil as reference. The Co K-edge X-ray absorption near-edge structure (XANES) shows that the absorption edge of Co<sub>SC</sub>-N-C exhibits a positive shift compared with that of Co foil, reflecting that the average valence state of Co atoms is at positive level and is higher than that in Co<sub>NP</sub>-N-C (Fig. 1d). The Fourier-transformed (FT) k<sup>3</sup>-weighted extended X-ray absorption fine structure (EXAFS) spectrum of the Co<sub>SC</sub>-N-C (Fig. 1e) shows two main peaks at about 1.5 Å and 2.2 Å, attributing to Co-N and Co-Co, respectively. In great contrast, only a strong Co-Co coordination is detected in Co<sub>NP</sub>-N-C, so that the Co atoms are present as nanoparticles in the carbon framework. The surface chemistry of different samples was further investigated by X-ray photoelectron spectroscopy (XPS, Supplementary Fig. 7). The coexistence of four different N species in different samples, namely pyridinic-N, pyrrolic-N, graphitic-N and N-oxides, was confirmed by the high-resolution N 1s spectra (Supplementary Fig. 8) [26,27]. The high-resolution Co 2p spectra (Supplementary Fig. 9) show higher valence states of Co in Co<sub>SC</sub>-N-C compared with Co<sub>NP</sub>-N-C [28,29], indicating the coordination of cobalt and nitrogen, which is in accordance with the XAFS responses. The XPS results and the XAFS responses are combined to confirm the existence of nitrogen-stabilized cobalt single clusters in Co<sub>SC</sub>-N-C. In addition, Co<sub>SC</sub>-N-C possesses a large surface area of 287.1 m<sup>2</sup> g<sup>-1</sup>, as

determined by the Brunauer-Emmett-Teller (BET) method (Supplementary Fig. 10).

## Electroreduction of N<sub>2</sub> to NH<sub>3</sub> on the Co<sub>SC</sub>-N-C catalyst

To evaluate the NRR activity of different samples, linear sweep voltammetry (LSV) curves were first measured (Supplementary Fig. 11). The current density difference between Ar and N<sub>2</sub> clearly affirms the contribution from the nitrogen reduction. Without cobalt sites, N-C exhibits the weakest NRR and hydrogen evolution reaction (HER) activity. While, compared with Co<sub>NP</sub>-N-C, the bigger current density gap between Ar and N<sub>2</sub> and lower HER current density of Co<sub>SC</sub>-N-C indicate that the introduction of cobalt single clusters leads to much more improved NRR activity and selectivity than those of the cobalt nanoparticles. Then, a quantified study of the NRR ability for different samples was carried out via chronoamperometry measurement using an H-shape electrochemical cell [30]. Here, the most rigorous experimental protocol was followed for reliable proof of the NRR performance [31]. The nitrogen gas was sufficiently purified before use to avoid the possible existence of NH<sub>3</sub> and NO<sub>x</sub>. Possible reduction products including NH<sub>3</sub> and N<sub>2</sub>H<sub>4</sub> were both tested (Supplementary Figs 12–15), whereas only NH<sub>3</sub> was detected in this work (Supplementary Fig. 16). Before the NRR test, several control experiments were first carried out to ensure that no contamination was present in the feeding gas or the equipment, and the carbon paper (CP) as current collector of the cathode did not have NRR activity, so that NH<sub>3</sub> could only be produced by N<sub>2</sub> reduction in the presence of catalyst (Fig. 2a). Detailed comparison of the NH<sub>3</sub> yield rates and corresponding Faradaic efficiencies of Co<sub>SC</sub>-N-C, Co<sub>NP</sub>-N-C and N-C under various applied potentials is displayed in Fig. 2b and c. Clearly, pristine N-C exhibits only negligible NRR performance. After incorporating cobalt single clusters, the Co<sub>SC</sub>-N-C, with an optimized loading of 0.5 mg cm<sup>-2</sup> (Supplementary Fig. 17), exhibits the highest NH<sub>3</sub> yield rate of 76.2 μg h<sup>-1</sup> mg<sub>cat.</sub><sup>-1</sup> at -0.2 V versus reversible hydrogen electrode (vs. RHE), far exceeding the peak value of Co<sub>NP</sub>-N-C (22.5 μg h<sup>-1</sup> mg<sub>cat.</sub><sup>-1</sup>) realized at an even more negative potential (-0.3 V vs. RHE). Notably, the maximal NRR Faradaic efficiency of Co<sub>SC</sub>-N-C is also obtained at -0.2 V vs. RHE (52.9%), which is more than one order of magnitude higher than the counterparts. Detailed chronoamperometry responses are shown in Supplementary Fig. 18. Also, the electrochemical active surface area (EASA) of each sample was determined by double-layer

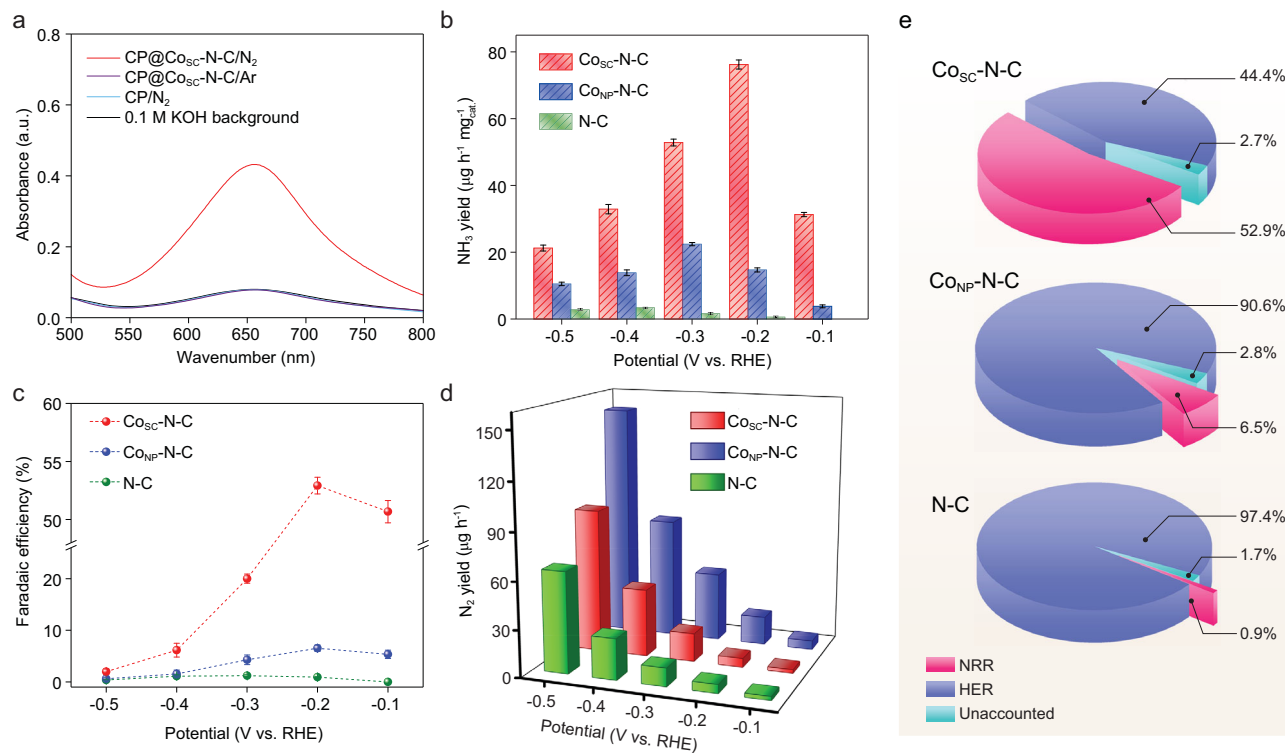


**Figure 2.** (a) The UV-vis absorption spectra of the electrolytes after electrolysis under different conditions. (b)  $\text{NH}_3$  yield rates and (c) corresponding Faradaic efficiencies at each given potential of  $\text{Co}_{\text{SC}}\text{-N-C}$ ,  $\text{Co}_{\text{NP}}\text{-N-C}$  and  $\text{N-C}$ . (d)  $\text{H}_2$  yield of  $\text{Co}_{\text{SC}}\text{-N-C}$ ,  $\text{Co}_{\text{NP}}\text{-N-C}$  and  $\text{N-C}$  at different potentials. The error bars correspond to the standard deviations of the obtained data over three separately conducted electrochemical measurements under the same conditions. (e) Selectivity of NRR and HER at  $-0.2$  V vs. RHE of different samples.

capacitance ( $C_{\text{dl}}$ , Supplementary Fig. 19). Expectedly, the surface-area-normalized ammonia production rate of  $\text{Co}_{\text{SC}}\text{-N-C}$  shows an obvious advantage over other samples (Supplementary Fig. 20). The NRR activity and selectivity of  $\text{Co}_{\text{SC}}\text{-N-C}$  remarkably stands at the top level of reported catalysts under mild conditions (Supplementary Table 1), and is thus of great significance in energy utilization. Based on the nitrogen temperature-programmed desorption ( $\text{N}_2\text{-TPD}$ ) spectra (Supplementary Fig. 21),  $\text{Co}_{\text{SC}}\text{-N-C}$  exhibits the strongest  $\text{N}_2$  adsorption ability, confirming that cobalt single clusters are superior nitrogen-adsorption active sites compared with cobalt nanoparticles or nitrogen-doped carbon [32]. The gradual decrease of the NRR Faradaic efficiency of  $\text{Co}_{\text{SC}}\text{-N-C}$  as the applied potential becomes more negative than  $-0.2$  V vs. RHE is mainly due to the increased HER [33], as evaluated by the gas chromatography (GC) responses (Fig. 2d and Supplementary Fig. 22). In terms of selectivity,  $\text{Co}_{\text{SC}}\text{-N-C}$  shows a much smaller proportion of the competing HER compared with  $\text{Co}_{\text{NP}}\text{-N-C}$  and  $\text{N-C}$ , and is more inclined to proceed NRR (Supplementary Fig. 23). Based on the above results,  $\text{Co}_{\text{SC}}\text{-N-C}$  has a prominent advantage in nitrogen reduction, especially at  $-0.2$  V vs. RHE (Fig. 2e and Supplementary Table 2).

Careful examination of the N source for produced  $\text{NH}_3$  is helpful in getting an in-depth understanding of the catalyzing mechanism. Thus, isotope-labeling experiments were systematically conducted [34–37]. The  $^{15}\text{N}_2$  gas was also sufficiently purified before use. As shown in the ultraviolet-visible (UV-vis) absorption spectra (Fig. 3a), no  $\text{NH}_3$  can be detected when  $^{15}\text{N}_2$  is fed unless an electrocatalytic potential was applied to the  $\text{Co}_{\text{SC}}\text{-N-C}$  working electrode. Then, the produced  $\text{NH}_3$  was distinguished using  $^1\text{H}$  nuclear magnetic resonance ( $^1\text{H}$  NMR) spectra (Fig. 3b). After a continuous electrolysis under  $-0.2$  V vs. RHE using  $^{15}\text{N}_2$  as feeding gas, only a doublet signal ( $\sim 73$  Hz) representing  $^{15}\text{NH}_4^+$  is detected in the spectra instead of the triplet signal ( $\sim 52$  Hz) of  $^{14}\text{NH}_4^+$ . When Ar was used for electrolysis, no  $\text{NH}_3$  signal was detected in the NMR spectrum, indicating the obtained ammonia is totally from the  $\text{N}_2$  electroreduction process. For accuracy of the performance data, NMR method was also employed for ammonia quantification (Fig. 3c and Supplementary Fig. 24). The  $\text{NH}_3$  yield rate and Faradaic efficiency obtained by quantitative  $^1\text{H}$  NMR and colorimetric method using both  $^{14}\text{N}_2$  and  $^{15}\text{N}_2$  exhibit good consistency (Fig. 3d), thus demonstrating the reliability of the experimental results.

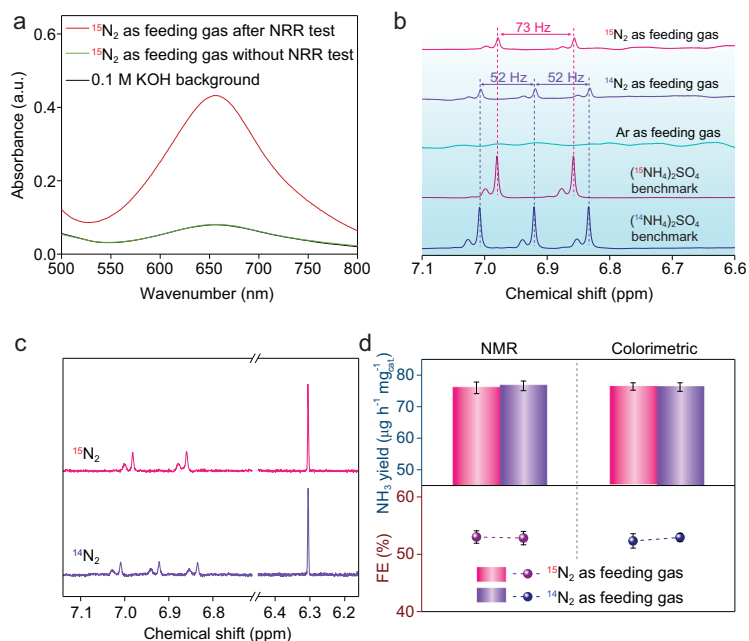


**Figure 3.** (a) The UV-vis absorption spectra of the electrolytes after electrolysis using  $^{15}\text{N}_2$  as feeding gas under different conditions. (b)  $^1\text{H}$  nuclear magnetic resonance (NMR) spectra of both  $^{14}\text{NH}_4^+$  and  $^{15}\text{NH}_4^+$  produced from the NRR using  $^{14}\text{N}_2$  and  $^{15}\text{N}_2$  as feeding gas, respectively. (c)  $^1\text{H}$  NMR spectra of the NRR product at  $-0.2$  V vs. RHE using NMR quantification method. (d) Comparison of  $\text{NH}_3$  yield rate and Faradaic efficiency for NRR at  $-0.2$  V vs. RHE using different quantification methods. The error bars correspond to the standard deviations of the obtained data over three separately conducted electrochemical measurements under the same conditions.

Stability is another vital parameter for an electrocatalyst. Thus, the durability of  $\text{Co}_{\text{SC}}\text{-N-C}$  was consecutively tested by electrolyzing at a constant potential of  $-0.2$  V vs. RHE for 10 cycles. The  $\text{Co}_{\text{SC}}\text{-N-C}$  catalyst can keep the superior Faradaic efficiency of  $\text{NH}_3$  production unchanged even after 10 cycles of continuous electrolysis (Supplementary Fig. 25), manifesting its broad prospect for practical applications. Simultaneously, TEM image, corresponding element maps and Raman spectra (Supplementary Figs 26 and 27) exhibit no variation in the morphology and structural properties of  $\text{Co}_{\text{SC}}\text{-N-C}$  after the NRR process. Its chemical state is also well maintained as confirmed by the high-resolution XPS spectra analyses (Supplementary Fig. 28), demonstrating that the  $\text{Co}_{\text{SC}}\text{-N-C}$  is robust enough for long-term NRR electrocatalysis.

### Computational studies

Computational studies on both thermodynamics and dynamics were carried out to investigate the mechanism of ammonia synthesis over the  $\text{Co}_{\text{SC}}\text{-N-C}$  catalyst. The thermodynamic process of different models was first studied by DFT calculations. As confirmed by catalyst characterizations, the cobalt

in  $\text{Co}_{\text{SC}}\text{-N-C}$  mainly exists as single clusters. Accordingly, several possible models of cobalt single cluster with different numbers of cobalt atoms on nitrogen-doped carbon ( $\text{Co}_x\text{-N}_4/\text{C}$ ,  $x = 2$  to 6) were systematically proposed, and pure nitrogen-doped carbon ( $\text{N}_4/\text{C}$ ) was also calculated for comparison (Supplementary Fig. 29). For  $\text{N}_4/\text{C}$ , the nitrogen adsorption is a strong endothermic process with a step-by-step uphill trend of Gibbs free energy (Supplementary Fig. 30). The introduction of cobalt single clusters is able to turn the nitrogen adsorption into exothermic process without energy barriers, suggesting that the cobalt single clusters are superior nitrogen-adsorption active sites. Notably, all of the structures with cobalt single clusters are able to alter the rate-determining step to the subsequent nitrogen hydrogenation with relatively small energy barriers (Supplementary Figs 31 and 32). Taking  $\text{Co}_4\text{-N}_4/\text{C}$  for example, as clearly shown in Fig. 4a, starting from a favored side-on mode  $\text{N}_2$  adsorption, the preferred NRR approach of  $\text{Co}_4\text{-N}_4/\text{C}$  is verified to be the associative alternating pathway instead of the associative distal pathway (Supplementary Fig. 33a). When chemically adsorbed on Co cluster,  $\text{N}_2$  is spontaneously activated and experiences a significant weakening of the  $\text{N}\equiv\text{N}$  bond due to the strong electron backdonation from the metal to the  $\text{N}_2$  antibonding orbitals, and the  $\text{N}_2$  dissociation becomes an exothermic process over the cobalt single cluster. In addition, the energy released from the  $\text{N}_2$  adsorption step greatly benefits the following  $\text{N}_2$  cleavage, according to the ‘hot atom’ mechanism [19,38]. Thus, the rate-determining step has been successfully shifted from the usual  $\text{N}_2$  activation to the subsequent hydrogenation with only a small energy barrier of 0.85 eV. In great contrast, without the Co single cluster, the  $\text{N}_4/\text{C}$  model not only suffers a severely endothermic  $\text{N}_2$  adsorption process, but also possesses high NRR rate-limiting barriers of 2.04 eV and 1.84 eV for the alternating and distal pathways, respectively, indicating a weak activity towards NRR (Fig. 4b and Supplementary Fig. 33b). On the other hand,  $\text{N}_2$  has priority in the adsorption competition with  $^*\text{H}$  on  $\text{Co}_4\text{-N}_4/\text{C}$ . As shown in Fig. 5a and b, the  $\text{N}_2$  chemisorption on  $\text{Co}_4\text{-N}_4/\text{C}$  is strongly exothermic ( $-0.82$  eV) with a step-by-step downhill trend of the Gibbs free energy, whereas the H chemisorption suffers an extremely high energy barrier of 2.53 eV due to the water dissociation process. Even if  $^*\text{H}$  is adsorbed, its desorption to form  $\text{H}_2$  is still an endothermic reaction (Supplementary Fig. 34), which is also beneficial to promoting the NRR Faradaic efficiency.

From a dynamic point of view, the  $\text{N}_2$  approaching process towards  $\text{Co}_4\text{-N}_4/\text{C}$  was then explored

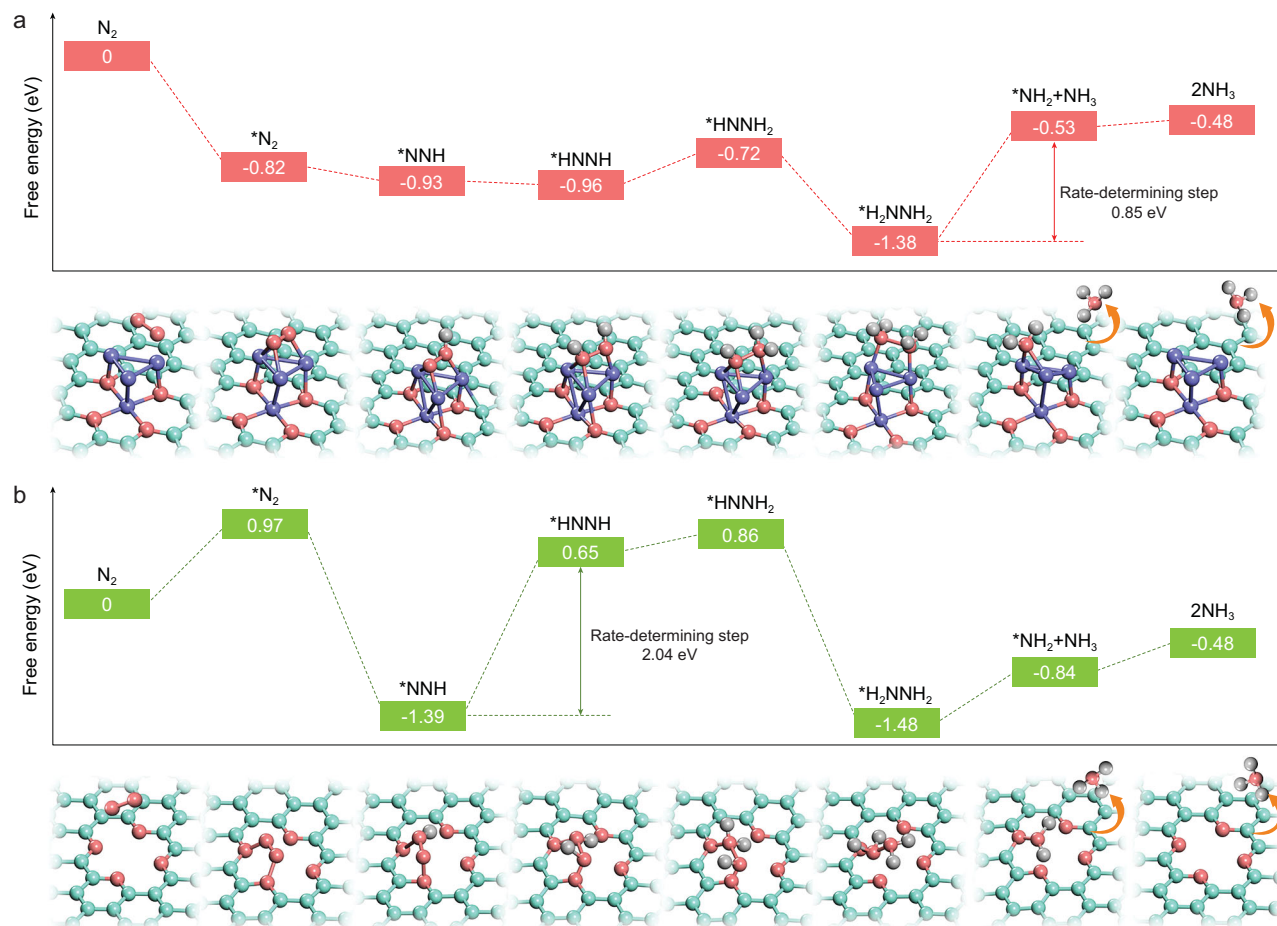


**Figure 4.** Free energy diagram and models represent the corresponding adsorbates on (a)  $\text{Co}_4\text{-N}_4/\text{C}$  and (b)  $\text{N}_4/\text{C}$  through the associative alternating pathway. The cyan, red, purple and gray spheres represent C, N, Co and H atoms, respectively.

by advanced sampling MD simulations. The system was set up by randomly placing 6  $\text{K}^+$ , 6  $\text{OH}^-$  and 3000 water molecules in the simulation box, with a  $\text{Co}_4\text{-N}_4/\text{C}$  model fixed perpendicular to the z-axis at the center of the simulation system. The  $\text{N}_2$  molecule initially located at 1.5 nm above the geometric center of the upper three Co atoms. Then, the  $\text{N}_2$  molecule was pulled towards the  $\text{Co}_4\text{-N}_4/\text{C}$  along the z-axis at a rate of  $0.01 \text{ nm ps}^{-1}$  under a harmonic force constant to generate configurations for umbrella-sampling (Fig. 5c). The potential of the mean force (PMF) as a function of distance and the corresponding snapshots (Fig. 5d and Supplementary Fig. 35) illustrate that the approaching process of  $\text{N}_2$  molecule is nearly barrierless with only a small energy hill at approximately 0.52 nm. This clearly indicates that the cobalt single cluster as active site is accessible to the  $\text{N}_2$  molecule, which can greatly promote the following  $\text{N}_2$  chemisorption, and is thus contributory to the entire NRR process. The above computational conclusions well explain the experimental

results, and further highlight the contribution of the cobalt single cluster as an important promoter for ambient  $\text{N}_2$  fixation.

## CONCLUSION

In summary, we have successfully altered the rate-determining step of ambient  $\text{NH}_3$  synthesis by deliberate introduction of cobalt single clusters as electron-donating promoter in nitrogen-doped carbon, and achieved outstanding ammonia yield rate of  $76.2 \mu\text{g h}^{-1} \text{ mg}_{\text{cat}}^{-1}$  and superior Faradaic efficiency of 52.9%. The  $\text{Co}_{\text{SC}}\text{-N-C}$  is steady enough for long-term NRR electrocatalysis with negligible decay of the amazingly high Faradaic efficiency through consecutive electrolysis recycle. The  $^{15}\text{N}$  isotopic labeling experiments and control experiments are combined to confirm that the N source of  $\text{N}_2$ -to- $\text{NH}_3$  conversion is completely from the feeding gas instead of any activated N species in the catalyst. First-principles simulations demonstrate a strong exothermic process of  $\text{N}_2$  chemisorption on the cobalt

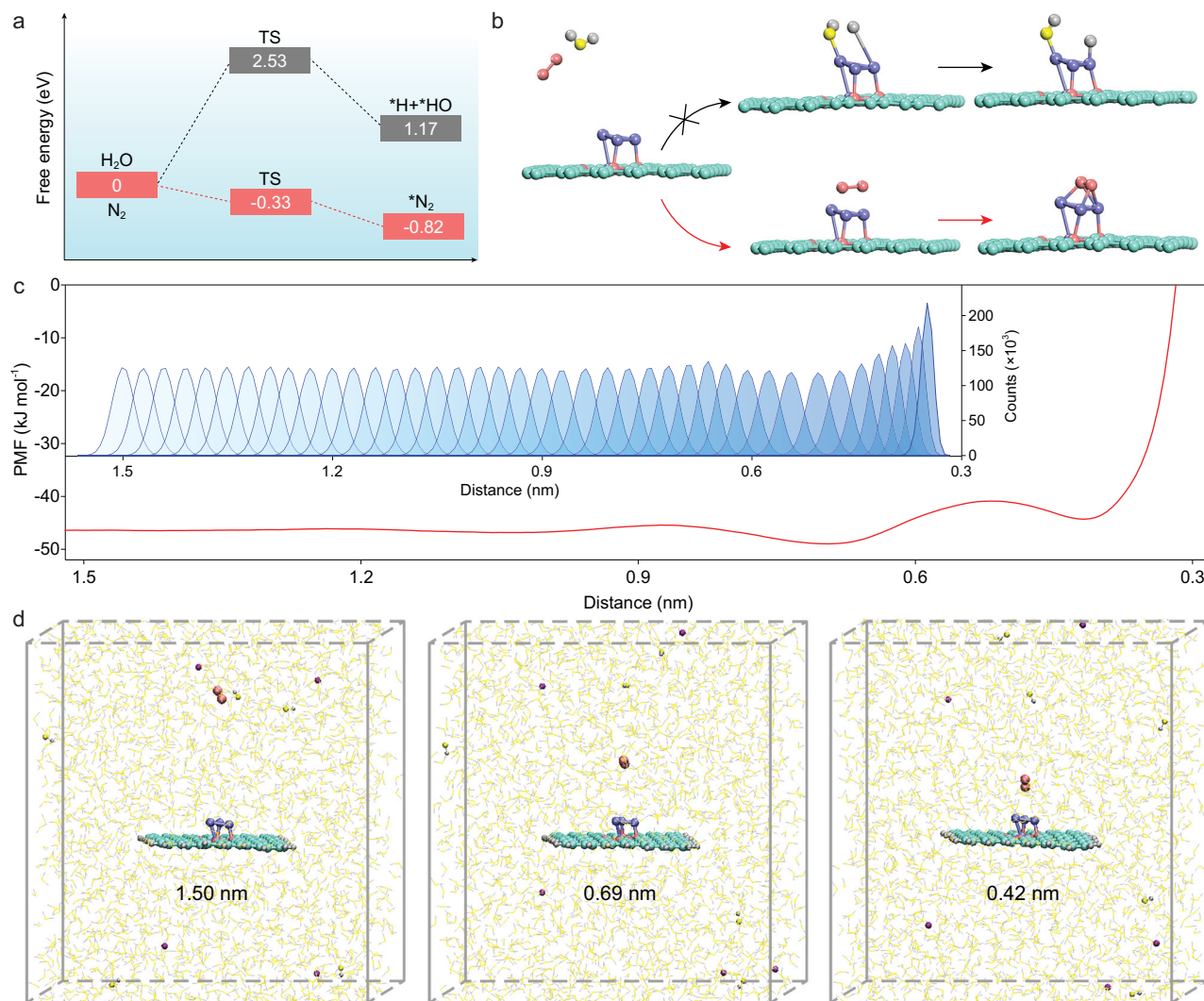


**Figure 5.** (a) Calculated free energy and (b) computational models of the transition state (TS) of hydrogen and nitrogen chemisorption on Co<sub>4</sub>-N<sub>4</sub>/C model. The cyan, red, purple, yellow and gray spheres represent C, N, Co, O and H atoms, respectively. (c) PMF for N<sub>2</sub> adsorption on the Co<sub>4</sub>-N<sub>4</sub> model in 0.1 M KOH; inset: complete histograms of all window umbrella sampling statistics used for calculation of the N<sub>2</sub> adsorption on the Co<sub>4</sub>-N<sub>4</sub> model. (d) Major part of the MD simulation snapshots at 1.50 nm, 0.69 nm and 0.42 nm, with N<sub>2</sub> (red spheres), H<sub>2</sub>O (yellow and gray sticks), OH<sup>-</sup> (yellow and gray spheres) and K<sup>+</sup> (wine red spheres).

single cluster site, which greatly promotes the following N<sub>2</sub> dissociation. The N<sub>2</sub> activation, therefore, becomes exothermic, and the rate-determining step has been successfully altered to the subsequent nitrogen hydrogenation. A smooth N<sub>2</sub> approaching process with almost no energy hill towards the catalyst paves the way for the N<sub>2</sub> mass transfer, as confirmed by the MD simulations. Our work overcomes the obstacle of ambient ammonia synthesis, and contributes to the guiding of future catalyst design for sustainable NRR systems.

## SUPPLEMENTARY DATA

Supplementary data are available at [NSR](https://doi.org/10.1093/nsr/nwaa136) online.

## FUNDING

This work was supported by the National Natural Science Foundation of China (21703149, 51622208, 51872193 and 5192500409) and the Natural Science Foundation of Jiangsu Province (BK20190827 and BK20181168).

## AUTHOR CONTRIBUTIONS

T.Q. conceived and designed this work. C.Y. supervised the project. S.L. prepared materials and performed the material characterizations and electrochemical measurements. S.L. and M.W. participated in analyzing the experimental results. H.J. conducted the theoretical calculations. X.S. offered help in the material characterizations. S.L. wrote this paper with feedback from the other

authors. All authors discussed the results and commented on the manuscript.

**Conflict of interest statement.** None declared.

## REFERENCES

- Gruber N and Galloway JN. An earth-system perspective of the global nitrogen cycle. *Nature* 2018; **451**: 293–6.
- Li X, Li T and Ma Y *et al.* Boosted electrocatalytic N<sub>2</sub> reduction to NH<sub>3</sub> by defect-rich MoS<sub>2</sub> nanoflower. *Adv Energy Mater* 2018; **8**: 1801357.
- Ali M, Zhou F and Chen K *et al.* Nanostructured photoelectrochemical solar cell for nitrogen reduction using plasmon-enhanced black silicon. *Nat Commun* 2016; **7**: 11335.
- van der Ham CJM, Koper MTM and Hetterscheid DGH. Challenges in reduction of dinitrogen by proton and electron transfer. *Chem Soc Rev* 2014; **43**: 5183–91.
- Shi M-M, Bao D and Wulan B-R *et al.* Au sub-nanoclusters on TiO<sub>2</sub> toward highly efficient and selective electrocatalyst for N<sub>2</sub> conversion to NH<sub>3</sub> at ambient conditions. *Adv Mater* 2017; **29**: 1606550.
- Licht S, Cui B and Wang B *et al.* Ammonia synthesis by N<sub>2</sub> and steam electrolysis in molten hydroxide suspensions of nanoscale Fe<sub>2</sub>O<sub>3</sub>. *Science* 2014; **345**: 637–40.
- Wang M, Liu S and Qian T *et al.* Over 56.55% Faradaic efficiency of ambient ammonia synthesis enabled by positively shifting the reaction potential. *Nat Commun* 2019; **10**: 341.
- Wang L, Xia M and Wang H *et al.* Greening ammonia toward the solar ammonia refinery. *Joule* 2018; **2**: 1055–74.
- Wang J, Yu L and Hu L *et al.* Ambient ammonia synthesis via palladium-catalyzed electrohydrogenation of dinitrogen at low overpotential. *Nat Commun* 2018; **9**: 1795.
- Li SJ, Bao D and Shi M-M *et al.* Amorphizing of Au nanoparticles by CeO<sub>x</sub>-RGO hybrid support towards highly efficient electrocatalyst for N<sub>2</sub> reduction under ambient conditions. *Adv Mater* 2017; **29**: 1700001.
- Zhang L, Ji X and Ren X *et al.* Electrochemical ammonia synthesis via nitrogen reduction reaction on a MoS<sub>2</sub> catalyst: theoretical and experimental studies. *Adv Mater* 2019; **30**: 1800191.
- Seh ZW, Kibsgaard J and Dickens CF *et al.* Combining theory and experiment in electrocatalysis: insights into materials design. *Science* 2017; **355**: eaad4998.
- Lv C, Yan C and Chen G *et al.* An amorphous noble-metal-free electrocatalyst enables N<sub>2</sub> fixation under ambient conditions. *Angew Chem Int Ed* 2018; **57**: 6073–6.
- Liu S, Wang M and Qian T *et al.* Facilitating nitrogen accessibility to boron-rich covalent organic frameworks via electrochemical excitation for efficient nitrogen fixation. *Nat Commun* 2019; **10**: 3898.
- Chen G-F, Ren S and Zhang L *et al.* Advances in electrocatalytic N<sub>2</sub> reduction-strategies to tackle the selectivity challenge. *Small Methods* 2019; **3**: 1800337.
- Qiu W, Xie XY and Qiu J *et al.* High-performance artificial nitrogen fixation at ambient conditions using a metal-free electrocatalyst. *Nat Commun* 2018; **9**: 3485.
- Guo C, Ran J and Vasileff A *et al.* Rational design of electrocatalysts and photo(electro)catalysts for nitrogen reduction to ammonia (NH<sub>3</sub>) under ambient conditions. *Energy Environ Sci* 2018; **11**: 45–56.
- Cui X, Tang C and Zhang Q. A review of electrocatalytic reduction of dinitrogen to ammonia under ambient conditions. *Adv Energy Mater* 2018; **8**: 1800369.
- Gong Y, Wu J and Kitano M *et al.* Ternary intermetallic LaCoSi as a catalyst for N<sub>2</sub> activation. *Nat Catal* 2018; **1**: 178–85.
- Légaré M-A, Bélanger-Chabot G and Dewhurst RD *et al.* Nitrogen fixation and reduction at boron. *Science* 2018; **359**: 896–900.
- Ma X-L, Liu J-C and Xiao H *et al.* Surface single-cluster catalyst for N<sub>2</sub>-to-NH<sub>3</sub> thermal conversion. *J Am Chem Soc* 2018; **140**: 46–9.
- Kitano M, Inoue Y and Yamazaki Y *et al.* Ammonia synthesis using a stable electride as an electron donor and reversible hydrogen store. *Nat Chem* 2012; **4**: 934–40.
- Kitano M, Kanbara S and Inoue Y *et al.* Electride support boosts nitrogen dissociation over ruthenium catalyst and shifts the bottleneck in ammonia synthesis. *Nat Commun* 2015; **6**: 6731.
- Wang P, Chang F and Gao W *et al.* Breaking scaling relations to achieve low-temperature ammonia synthesis through LiH-mediated nitrogen transfer and hydrogenation. *Nat Chem* 2017; **9**: 64–70.
- Inoue Y, Kitano M and Kishida K *et al.* Efficient and stable ammonia synthesis by self-organized flat Ru nanoparticles on calcium amide. *ACS Catal* 2016; **6**: 7577–84.
- Fei H, Dong J and Arellano-Jiménez A *et al.* Atomic cobalt on nitrogen-doped graphene for hydrogen generation. *Nat Commun* 2015; **6**: 8668.
- Fu J, Hassan FM and Li J *et al.* Flexible rechargeable zinc-air batteries through morphological emulation of human hair array. *Adv Mater* 2016; **28**: 6421–8.
- Jin H, Wang J and Su D *et al.* In situ cobalt–cobalt oxide/N-doped carbon hybrids as superior bifunctional electrocatalysts for hydrogen and oxygen evolution. *J Am Chem Soc* 2015; **137**: 2688–94.
- Guan C, Sumboja A and Zang W *et al.* Decorating Co/CoN<sub>x</sub> nanoparticles in nitrogen-doped carbon nanoarrays for flexible and rechargeable zinc-air batteries. *Energy Storage Mater* 2019; **16**: 243–50.
- Bao D, Zhang Q and Meng F-L *et al.* Electrochemical reduction of N<sub>2</sub> under ambient conditions for artificial N<sub>2</sub> fixation and renewable energy storage using N<sub>2</sub>/NH<sub>3</sub> cycle. *Adv Mater* 2017; **29**: 1604799.
- Andersen SZ, Čolić V and Yang S *et al.* A rigorous electrochemical ammonia synthesis protocol with quantitative isotope measurements. *Nature* 2019; **570**: 504–8.
- Zhang L, Ding L-X and Chen G-F *et al.* Ammonia synthesis under ambient conditions: selective electroreduction of dinitrogen to ammonia on black phosphorus nanosheets. *Angew Chem Int Ed* 2019; **58**: 2612–6.



33. Chen H, Ding L-X and Chen G-F *et al.* Molybdenum carbide nanodots enable efficient electrocatalytic nitrogen fixation under ambient conditions. *Adv Mater* 2018; **30**: 1803694.
34. Chen H, Cui P and Wang F *et al.* High efficiency electrochemical nitrogen fixation achieved on a low-pressure reaction system by changing chemical equilibrium. *Angew Chem Int Ed* 2019; **58**: 15541–7.
35. Luo Y, Chen G-F and Ding L *et al.* Efficient electrocatalytic N<sub>2</sub> fixation with MXene under ambient conditions. *Joule* 2019; **3**: 279–89.
36. Chen G-F, Cao X and Wu S *et al.* Ammonia electrosynthesis with high selectivity under ambient conditions via a Li<sup>+</sup> incorporation strategy. *J Am Chem Soc* 2017; **139**: 9771–4.
37. Zhou F, Azofra LM and Ali M *et al.* Electro-synthesis of ammonia from nitrogen at ambient temperature and pressure in ionic liquids. *Energy Environ Sci* 2017; **10**: 2516–20.
38. Wang J, Zhang L and Zeng Q *et al.* Adsorption of atomic and molecular oxygen on 3C-SiC(111) and (111) surfaces: a first-principles study. *Phys Rev B* 2009; **79**: 125304.